Thermodynamically admissible boundary conditions for the regularized 13 moment equations

Anirudh Singh Rana and Henning Struchtrup

Citation: Physics of Fluids **28**, 027105 (2016); doi: 10.1063/1.4941293
View online: http://dx.doi.org/10.1063/1.4941293
View Table of Contents: http://scitation.aip.org/content/aip/journal/pof2/28/2?ver=pdfcov
Published by the AIP Publishing

PHYSICS OF FLUIDS **28**, 027105 (2016)

Thermodynamically admissible boundary conditions for the regularized 13 moment equations

Anirudh Singh Rana[1,a)] and Henning Struchtrup[2,b)]
[1]*Department of Mechanical and Aerospace Engineering, Gyeongsang National University, Jinju, Gyeongnam 52828, South Korea*
[2]*Department of Mechanical Engineering, University of Victoria, Victoria, British Columbia V8W 2Y2, Canada*

(Received 21 September 2015; accepted 20 January 2016; published online 5 February 2016)

A phenomenological approach to the boundary conditions for linearized R13 equations is derived using the second law of thermodynamics. The phenomenological coefficients appearing in the boundary conditions are calculated by comparing the slip, jump, and thermal creep coefficients with linearized Boltzmann solutions for Maxwell's accommodation model for different values of the accommodation coefficient. For this, the linearized R13 equations are solved for viscous slip, thermal creep, and temperature jump problems and the results are compared to the solutions of the linearized Boltzmann equation. The influence of different collision models (hard-sphere, Bhatnagar–Gross–Krook, and Maxwell molecules) and accommodation coefficients on the phenomenological coefficients is studied. © *2016 AIP Publishing LLC.* [http://dx.doi.org/10.1063/1.4941293]

I. INTRODUCTION

Transport mechanisms in a gas under rarefied conditions pose unique challenges in present fluid mechanics. Such rarefied conditions occur, for example, in micro-electro-mechanical systems (MEMS), and high vacuum systems, where the dimensions of the devices are comparable to the mean free path of the gas molecules.[11,20] Accordingly, the degree of rarefaction in a gas is characterized by the Knudsen number, Kn, which is defined as the ratio of the molecular mean free path to the macroscopic length scale. Based on the value of the Knudsen number, the gas flow can be classified into four regimes: hydrodynamic regime ($\mathrm{Kn} \lesssim 0.001$), slip flow regime ($0.001 \lesssim \mathrm{Kn} \lesssim 0.01$), transition regime ($0.01 \lesssim \mathrm{Kn} \lesssim 10$), and free molecular flow regime ($10 \lesssim \mathrm{Kn}$).[11,20] It is commonly accepted that the classical description based on the Navier-Stokes and Fourier (NSF) equations is applicable only for the hydrodynamic flow regime.[13,38,55] For flows outside the hydrodynamic regime, many interesting rarefaction effects are observed, such as velocity slip and temperature jump at the walls,[24,38,46] Knudsen layers,[13,23,38] transpiration flow,[13,25,38] thermal stress,[30,38] and heat flux without temperature gradients.[27,31] These effects are termed as non-equilibrium effects and they cannot be described by the classical NSF equations. The range of validity of the NSF equations may further be extended to the slip flow regime by applying appropriate slip and jump boundary conditions to model the velocity slip and temperature jump at the walls, as well as transpiration flows.[59] However, they still cannot describe the Knudsen layers and other rarefaction effects.

A fully detailed description of the gas flow in all flow regimes is offered by the Boltzmann equation, which solves for the microscopic distribution function of the gas particles.[2,6] The solution of the Boltzmann equation is usually cumbersome, and computationally expensive. In macroscopic models, on the other hand, the behavior of a gas is described through physical quantities such as

a)Electronic mail: anirudh@uvic.ca
b)Electronic mail: struchtr@uvic.ca

mass density, temperature, velocity, heat flux, stress tensor, and so on. The goal of these macroscopic transport equations is to reduce the high dimensional phase space of the particle description to a low-dimensional continuum model by relating the physical quantities to moments of the distribution function.

Macroscopic equations are obtained by an asymptotic reduction of the Boltzmann equation at different levels of approximation and accuracy.[13,38,41] Conventionally, these equations are derived with either the Chapman-Enskog (CE) expansion method[8] or Grad's moment method.[14,15] The NSF equations can be obtained from the first order CE expansion of the Boltzmann equation. The second and third order CE expansions result in the Burnett and super-Burnett equations, respectively.[8,41] While the Burnett-type equations can describe rarefaction effects in the lower transition regime ($\mathrm{Kn} \lesssim 1$) with reasonable accuracy,[1] they suffer from instabilities for time-dependent problems.[3] Several modified forms of the Burnett equations have been suggested in the literature that are stable;[4,5,19,37] however, at present, no boundary conditions are available for any of these sets of equations. The 13 moment equations, obtained via Grad's moment method, are linearly stable but due to their hyperbolic character, Grad's 13 (G13) moment equations produce unphysical sub-shocks for high speed flows ($\mathrm{Ma} \gtrsim 1.65$).[57] Furthermore, in Grad's method, the number of moments is arbitrary, and therefore it is difficult to know *a priori* which sets of moments should be considered for a given process.

The regularized 13 (R13) moment equations, obtained by means of the order of magnitude method,[40] provide a clear relation between Knudsen number and the appropriate set of moment to be considered, as seen in Refs. 40 and 44 and also Ref. 41. In Ref. 41, it was shown that the G13 equations are of second order in the Knudsen number, while the R13 equations are of third order consequently, the Burnett and super-Burnett equations can be obtained by CE expansion of the R13 equations. The R13 equations are always linearly stable and give smooth shock structures for all Mach numbers, particularly, in good agreement with kinetic theory for $\mathrm{Ma} \lesssim 3$.[52]

The macroscopic boundary conditions (MBCs) for the R13 equations were already derived in Refs. 16 and 53, by introducing the Grad's 26 moment closure in Maxwell's accommodation model. It turned out that the original nonlinear R13 equations require more boundary conditions than those required for the linearized R13 equations, and this issue was discussed in Refs. 31 and 53. In Refs. 31 and 32, we used order of magnitude arguments to rewrite the non-linear part of the R13 equations such that the third order accuracy was maintained, but linear and nonlinear R13 equations require the same number of boundary conditions. Recently, the R13 equations for the hard sphere (HS) gas, gas-mixtures, and for polyatomic gases were derived in Refs. 47, 18, and 29, respectively.

Taheri *et al*. considered in Refs. 48–51 the closed-form solutions of the linearized R13 equations to several boundary value problems using MBC, which were qualitatively in good agreement with the reference solutions. In Ref. 50, the breakdown of the Onsager symmetry relations[33,34] was reported for pressure-driven and thermally driven rarefied gas flows in long capillaries using extended macroscopic models. It was shown that the linearized R13 equations obey (approximately) the Onsager reciprocity relation for moderate Knudsen numbers, $\mathrm{Kn} \lesssim 0.25$.

Young in Ref. 58 calculated the Knudsen layers and jump coefficients using linearized G13 equations and R13 equations. He showed that when compared with the direct solutions of the Boltzmann equation, the R13 equations with the MBC underpredict the velocity slip, thermal creep, and temperature jump coefficients by about 10%.

In the present paper, we shall address two issues regarding the violation of Onsager reciprocity relations[50] and the underprediction of the slip, jump, and creep coefficients by MBC for R13 equations.[58] First, we shall derive phenomenological boundary conditions (PBCs) for the R13 equations, which are thermodynamically admissible for all processes. Furthermore, the phenomenological coefficients in these boundary conditions are obtained such that the R13 equation gives correct velocity slip, thermal creep, and temperature jump coefficients in the bulk (i.e., outside of the Knudsen layers[46]). Earlier, in Ref. 53, Torrilhon and Struchtrup introduced *ad hoc* coefficients in the boundary conditions, so that an overall agreement with DSMC solutions was achieved. The reason for these corrections, as discussed in Ref. 53, is that the R13 equations cannot describe Knudsen layers completely, due to the lack of sublayer contributions from higher moments, see also Refs. 41 and 46. In the case of NSF, where Knudsen layers are completely absent, it is well known

that the slip and jump boundary conditions must be modified with artificial coefficients known as the slip and jump corrections, see Ref. 59. However, the extended moment equations, such as R13 equations, contain additional higher order moments and their respective boundary conditions, and without any physical meaning associated with these additional moments, a rational procedure to find corrected coefficients is required.

A phenomenological model of the wall boundary was presented in Ref. 45, which laid the foundation of the present work. To generalize the procedure in Ref. 45, in this paper, we consider the coupling between the cross terms of the same tensorial structure (i.e., the Curie principle).[9] When such coupling is considered, the resulting PBCs assume the same tensorial form as the MBC obtained via Grad's 26 moment closure in the Maxwell accommodation model,[53] with additional coefficients (Onsager coefficients). This allows us to identify and estimate the values for the Onsager coefficients in phenomenological boundary conditions. The presented theory gives thermodynamical restrictions on these coefficients. Furthermore, we revisit the Onsager symmetry using the linearized R13 equations and show that the violation of the Onsager symmetry relations as reported in Ref. 50 is due to the use of macroscopic boundary conditions, while the phenomenological boundary conditions obtained in this article comply with the Onsager symmetry relations for all Knudsen numbers.

The rest of the paper is organized as follows: The linearized R13 equations and their extended entropy law are summarized in Sec. II. The phenomenological boundary conditions for the linearized R13 equations are presented in Sec. III. To obtain some insight into the phenomenological coefficients appearing in the boundary conditions, in Sec. IV, we estimate the phenomenological coefficients by comparing the phenomenological boundary conditions with the macroscopic boundary conditions obtained from the Grad's closure. The breakdown of the Onsager symmetry relations for macroscopic boundary conditions is briefly examined in Sec. IV B. In Sec. V, the phenomenological coefficients are re-evaluated by comparing the slip, jump, and creep coefficients with the linearized Boltzmann solutions for different values of the accommodation coefficient. Our conclusions are reported in Sec. VI. The first two Appendices A and B list the normal-tangential decompositions for the tensors and the integration constants, respectively. Appendix C provides details regarding the derivation of phenomenological boundary conditions.

II. LINEARIZED EQUATIONS AND DIMENSIONLESS VARIABLES

We shall only consider flow conditions where the deviations from a constant equilibrium state, given by the reference mass density ρ_0 and the reference temperature T_0, are small. Thereby, the governing equations can be linearized with respect to the reference equilibrium rest state. Also the model will be put into dimensionless form using non-dimensional quantities, defined as

$$\begin{aligned} \hat{x}_i &= \frac{x_i}{L}, & \hat{\rho} &= \frac{\rho}{\rho_0}, & \hat{T} &= \frac{T}{T_0}, & \hat{p} &= \frac{p}{p_0}, \\ \hat{t} &= t\frac{L}{\sqrt{\mathrm{R}T_0}}, & \hat{v}_i &= \frac{v_i}{\sqrt{\mathrm{R}T_0}}, & \hat{\sigma}_{ij} &= \frac{\sigma_{ij}}{\rho_0 \mathrm{R}T_0}, & \hat{q}_i &= \frac{q_i}{\rho_o \sqrt{\mathrm{R}T_0}^3}, \end{aligned} \tag{1}$$

where L is a reference length and R is the gas constant. The hat over quantities indicates the corresponding non-dimensional quantity. For brevity, the hats will be removed hereafter, and unless otherwise stated, all variables will be given in non-dimensional form. The dimensionless R13 equations, after linearization, are written through conservation laws of mass, momentum, and energy, that are

$$\frac{D\rho}{Dt} + \frac{\partial v_k}{\partial x_k} = 0, \tag{2a}$$

$$\frac{Dv_i}{Dt} + \frac{\partial \sigma_{ik}}{\partial x_k} + \frac{\partial p}{\partial x_i} = F_i, \tag{2b}$$

$$\frac{3}{2}\frac{DT}{Dt} + \frac{\partial v_k}{\partial x_k} + \frac{\partial q_k}{\partial x_k} = 0, \tag{2c}$$

TABLE I. Burnett coefficients for Maxwell molecules (MMs), BGK model, and hard spheres (HS).

	ϖ_2	$\varpi_3 = \theta_4$	θ_2
MM	2	3	$\frac{45}{8}$
BGK	2	2	$\frac{5}{2}$
HS	2.027 74	2.421 13	5.819 45

where F_i is the dimensionless body force. The pressure is given by $p = \rho T$ (or $p = 1 + \rho + T$ after linearization), due to the assumption of ideal gas. The balance equations (linearized) for the stress tensor, σ_{ij}, and heat flux vector, q_i, are given as[41]

$$\frac{D\sigma_{ij}}{Dt} + \frac{4}{5}\mathrm{Pr}\frac{\varpi_3}{\varpi_2}\frac{\partial q_{\langle i}}{\partial x_{j\rangle}} + \frac{\partial m_{ijk}}{\partial x_k} = -\frac{2}{\varpi_2}\frac{1}{\mathrm{Kn}}\left[\sigma_{ij} + 2\mathrm{Kn}\frac{\partial v_{\langle i}}{\partial x_{j\rangle}}\right] \text{ and} \tag{3a}$$

$$\frac{Dq_i}{Dt} + \frac{5}{4\,\mathrm{Pr}}\frac{\theta_4}{\theta_2}\frac{\partial \sigma_{ik}}{\partial x_k} + \frac{1}{2}\frac{\partial R_{ik}}{\partial x_k} + \frac{1}{6}\frac{\partial \Delta}{\partial x_i} = -\frac{1}{\theta_2}\frac{5}{2\,\mathrm{Pr}}\frac{1}{\mathrm{Kn}}\left[q_i + \frac{5}{2\,\mathrm{Pr}}\mathrm{Kn}\frac{\partial T}{\partial x_i}\right], \tag{3b}$$

respectively. Here, ϖ_i, θ_i are the Burnett coefficients and Pr denotes the Prandtl number. These depend upon the choice of intermolecular potential function appearing in Boltzmann's collision integral.[8,41] Values of these coefficients for inverse-power potentials (i.e., the molecules repelling each other with an intermolecular force $\propto r^{-\nu}$) can be found in Table I.[41]

In addition to the stress tensor, σ_{ij}, and the heat flux vector, q_i, Equations (3) contain higher order moments, i.e., m_{ijk}, R_{ik}, and Δ. For first order models, it is sufficient to consider only the terms on the right-hand side of Equations (3), which gives the linearized laws of Navier-Stokes and Fourier. For Maxwell molecules (MMs), i.e., the molecules repelling each other with an intermolecular force $\propto r^{-5}$, the second order equations turn out to be the original G13 moment equations and give $m_{ijk} = 0$, $R_{ij} = 0$, and $\Delta = 0$. At third order accuracy, one arrives at the regularized 13 moment equations, see Ref. 41 and also Refs. 42 and 47. After linearization, they read

$$m_{ijk} = -\frac{3\mathrm{Kn}}{\mathrm{Pr_M}}\frac{\partial \sigma_{\langle ij}}{\partial x_{k\rangle}}, R_{ij} = -\frac{28}{5}\frac{\mathrm{Kn}}{\mathrm{Pr_R}}\frac{\partial q_{\langle i}}{\partial x_{j\rangle}}, \text{ and } \Delta = -\frac{8\mathrm{Kn}}{\mathrm{Pr}_\Delta}\frac{\partial q_k}{\partial x_k}, \tag{4}$$

where transport coefficients Pr, $\mathrm{Pr_R}$, $\mathrm{Pr_M}$, and Pr_Δ are given in Table II. Constitutive relations (4) complete conservation laws (2) and balance equations (3) to form the linear R13 equations.

As shown in Ref. 45, the linear R13 equations are accompanied by an entropy law given as

$$\frac{D\eta}{Dt} + \frac{\partial \Psi_k}{\partial x_k} = \Sigma, \tag{5}$$

where $\eta\,(=s/\mathrm{R})$ is the dimensionless entropy density, Ψ_k is entropy flux, and Σ is the entropy production rate. For the linear R13 equations, the entropy is a quadratic convex function, given as

$$\eta = \eta_0 - \frac{\rho^2}{2} - \frac{3}{4}T^2 - \frac{v^2}{2} - \frac{\varpi_2}{8}\sigma^2 - \frac{2\theta_2}{25}\mathrm{Pr}^2 q^2, \tag{6}$$

and the entropy flux and entropy generation rate read

TABLE II. Transport coefficients for Maxwell molecules (MMs), Bhatnagar–Gross–Krook (BGK), and Hard-Sphere (HS) collision models.

	Pr	$\mathrm{Pr_R}$	$\mathrm{Pr_M}$	Pr_Δ
MM	2/3	7/6	3/2	2/3
BGK	1	1	1	1
HS	0.6609	1.3307	1.3951	0.9025

$$\Psi_k = -(\rho + T)\, v_k - v_i \sigma_{ik} - T q_k - \frac{\varpi_3}{5} \Pr\, q_i \sigma_{ik} - \frac{\varpi_2}{4} \sigma_{ij} m_{ijk} - \frac{2\theta_2}{25} \Pr^2 \left(q_i R_{ik} + \frac{\Delta}{3} q_k \right), \quad (7a)$$

$$\Sigma = \frac{\sigma_{ij}\sigma_{ij}}{2\mathrm{Kn}} + \frac{2\Pr}{5\mathrm{Kn}} q^2 - \frac{\varpi_2}{4} m_{ijk} \frac{\partial \sigma_{ij}}{\partial x_k} - \frac{2\theta_2}{25} \Pr^2 R_{ik} \frac{\partial q_i}{\partial x_k} - \frac{2\theta_2}{75} \Pr^2 \Delta \frac{\partial q_k}{\partial x_k}, \quad (7b)$$

respectively. Hence, R13 constitutive relations (4) give $\Sigma \geq 0$, for any thermodynamic process.

III. PHENOMENOLOGICAL BOUNDARY CONDITIONS FOR THE LINEARIZED R13 EQUATIONS

Integrating entropy balance equation (5) directly on the interface and using Gauss's theorem, we readily find that the entropy production density on an infinitesimal surface element is equal to the difference between the entropy fluxes into and out of the surface. For the wall in the rest frame, the local entropy production (per unit surface of the wall) reads

$$\Sigma_W = \left(\Psi_k - \Psi_k^W \right) n_k, \quad (8)$$

where n_k denotes the components of the unit normal vector of the wall pointing toward the gas and Ψ_k^W denotes the non-convective entropy flux from the wall. The entropy flux Ψ_k in (8) is given from Equation (7a). For a gas-wall interface, the jump conditions of mass and energy at the impermeable boundary are written as[45]

$$\left(v_k - v_k^W \right) n_k = 0, \Psi_k^W = -T^W q_k. \quad (9)$$

Here, v_k^W and T^W denote the velocity and temperature of the wall, respectively. We use relations (9) to eliminate Ψ_k^W in Equation (8). This yields the entropy production per unit surface area as

$$\Sigma_W^{\mathrm{LR13}} = \left(-\mathcal{V}_i \sigma_{ik} - \mathcal{T} q_k - \frac{\varpi_3}{5} \Pr\, q_i \sigma_{ik} - \frac{\varpi_2}{4} \sigma_{ij} m_{ijk} - \frac{2\theta_2}{25} \Pr^2 \left(q_i R_{ik} + \frac{\Delta}{3} q_k \right) \right) n_k, \quad (10)$$

where $\mathcal{V}_k = v_k - v_k^W$ and $\mathcal{T} = T - T^W$ are velocity slip and temperature jump, respectively. It is convenient to decompose the right hand side in Equation (10) into the normal and tangential components of the vectors $\mathcal{V}_i$ and q_i and tensors σ_{ij}, R_{ij}, and m_{ijk} (see Appendix A for the explicit expressions). In this case, Equation (10) simplifies to

$$\begin{aligned} \Sigma_W^{\mathrm{LR13}} = & -q_n \left[\mathcal{T} + \frac{\varpi_3}{5} \Pr\, \sigma_{nn} + \frac{2\theta_2}{25} \Pr^2 \left(R_{nn} + \frac{\Delta}{3} \right) \right] - m_{nnn} \left[\frac{3\varpi_2}{8} \sigma_{nn} \right] \\ & - \bar{\sigma}_{nk} \left[\mathcal{V}_k + \frac{\varpi_3}{5} \Pr\, \bar{q}_k + \frac{\varpi_2}{2} \bar{m}_{nnk} \right] - \bar{R}_{nk} \left[\frac{2\theta_2}{25} \Pr^2 \bar{q}_k \right] - \widetilde{m}_{nij} \left[\frac{\varpi_2}{4} \widetilde{\sigma}_{ij} \right]. \end{aligned} \quad (11)$$

In the last equation, subscripts n indicate the normal components of a tensor, and there is no summation implied for repeated indices. As the definitions Appendix A show, in Equation (11), q_n, σ_{nn}, m_{nnn}, etc., are the rank zero tensors (i.e., scalars), $\bar{\sigma}_{nk}$, $\bar{q}_k$, $\bar{m}_{nnk}$, $\bar{R}_{nk}$, etc., are the rank one tensors (i.e., vectors), and finally $\widetilde{m}_{nij}$, $\widetilde{\sigma}_{ij}$, etc., are the rank two tensors (i.e., matrix). Therefore, first two terms in (11) are multiplication of scalers, third and fourth terms are the dot product of vectors, and the last term is the dot product of two matrices. Furthermore, in Equation (11), the fluxes with the odd degree in n (i.e., q_n, m_{nnn}, $\bar{\sigma}_{nk}$, $\bar{R}_{nk}$, $\widetilde{m}_{nij}$) are identified as the unknowns and the even moments as their driving forces (i.e., the expressions in square brackets). This is motivated from the observation of Grad which states that at the boundary only odd fluxes need to be prescribed.[14] From Equation (11), a positive entropy production can be achieved by writing the unknown boundary values for the odd moments proportional to their driving forces.[10,21] Thereby, we find the phenomenological boundary conditions for the linear R13-moment equations as (see Appendix C for the details)

$$\bar{\sigma}_{nk} = -\varsigma_0 \left[\mathcal{V}_k + \frac{\varpi_3 \Pr}{5} \bar{q}_k + \frac{\boldsymbol{\varpi_2}}{\boldsymbol{2}} \bar{\boldsymbol{m}}_{\boldsymbol{nnk}} \right] + \varsigma_1 \frac{2\theta_2}{25} \Pr^2 \bar{q}_k, \quad (12a)$$

$$\bar{R}_{nk} = \varsigma_1 \left[\mathcal{V}_k + \frac{\varpi_3 \Pr}{5} \bar{q}_k + \frac{\boldsymbol{\varpi_2}}{\boldsymbol{2}} \bar{\boldsymbol{m}}_{\boldsymbol{nnk}} \right] - \varsigma_2 \frac{2\theta_2}{25} \Pr^2 \bar{q}_k, \quad (12b)$$

$$q_n = -\tau_0 \left[\mathcal{T} + \frac{\varpi_3 \mathrm{Pr}}{5} \sigma_{nn} + \frac{\boldsymbol{2\theta_2 Pr^2}}{\boldsymbol{25}} \left(\boldsymbol{R_{nn}} + \frac{\boldsymbol{\Delta}}{\boldsymbol{3}} \right) \right] + \frac{3\tau_1 \varpi_2 \sigma_{nn}}{8}, \tag{12c}$$

$$m_{nnn} = \tau_1 \left[\mathcal{T} + \frac{\varpi_3 \mathrm{Pr}}{5} \sigma_{nn} + \frac{\boldsymbol{2\theta_2 Pr^2}}{\boldsymbol{25}} \left(\boldsymbol{R_{nn}} + \frac{\boldsymbol{\Delta}}{\boldsymbol{3}} \right) \right] - \frac{3\tau_2 \varpi_2 \sigma_{nn}}{8}, \tag{12d}$$

$$\widetilde{m}_{nij} = -\tau_3 \frac{\varpi_2}{4} \widetilde{\sigma}_{ij}. \tag{12e}$$

Here, the matrices

$$\varsigma_{ij} = \begin{bmatrix} \varsigma_0 & -\varsigma_1 \\ -\varsigma_1 & \varsigma_2 \end{bmatrix}, \tau_{ij} = \begin{bmatrix} \tau_0 & -\tau_1 \\ -\tau_1 & \tau_2 \end{bmatrix} \tag{13}$$

are any arbitrary symmetric non-negative definite matrices of Onsager coefficients and τ_3 is an arbitrary non-negative coefficient. The significance of the underlined terms in Eqs. (12) will be discussed in Sec. IV A.

IV. DETERMINATION OF PHENOMENOLOGICAL COEFFICIENTS

The phenomenological coefficients, ς_i and τ_i, appearing in PBC (12) depend on the microscopic interaction between gas particles and the wall. Due to the complexity of gas-wall interactions, it is quite common in kinetic theory to use simplified microscopic gas-wall interaction models which are determined by only a few parameters, typically known as accommodation coefficients.[7,26] Best known is Maxwell accommodation model, which uses only one single accommodation coefficient.[26] In this section, we shall estimate the phenomenological coefficients corresponding to the Maxwell accommodation model. In Secs. V A and V B, we shall investigate the effects of the phenomenological coefficients on the slip and jump coefficients and match them with more accurate solutions obtained from the linearized Boltzmann equation.

A. Macroscopic boundary conditions from Maxwell accommodation model

For the Maxwell accommodation model, the velocity distribution function $\tilde{f}(c)$ in an infinitesimal neighborhood of the wall is given as

$$\tilde{f}(c_i) = \begin{cases} \chi f_W(c_i) + (1-\chi) f^{(*)}(c_i) & n_k \left(c_k - v_k^W \right) \geq 0 \\ f(c_i) & n_k \left(c_k - v_k^W \right) < 0 \end{cases}, \tag{14}$$

where the accommodation coefficient $\chi \in [0,1]$ gives the fraction of the particles coming from the wall that have been diffused and reflected into the gas with a normal distribution $f_W\left(v_k^W; T^W\right)$. In Eq. (14), the particles that hit the wall are described by the gas distribution function f, and the distribution function of specularly reflected particles $f^{(*)}$ is obtained by reversing the sign of normal component of the microscopic velocities. In order to evaluate the macroscopic boundary conditions, the gas distribution f in (14) must be approximated. In Ref. 16, Gu and Emerson used Grad's 26 moment distribution function to approximate f in (14) to obtain MBC. Subsequently, Torrilhon and Struchtrup[53] and Taheri *et al.*[31] extended and refined these boundary conditions for the R13 equations. The macroscopic boundary conditions, after linearization, read

$$\bar{\sigma}_{nk} = -\sqrt{\frac{2}{\pi}} \frac{\chi}{2-\chi} \left[\mathcal{V}_k + \frac{1}{5} \bar{q}_k + \frac{\boldsymbol{1}}{\boldsymbol{2}} \bar{\boldsymbol{m}}_{\boldsymbol{nnk}} \right], \tag{15a}$$

$$\bar{R}_{nk} = \sqrt{\frac{2}{\pi}} \frac{\chi}{2-\chi} \left[\mathcal{V}_k - \frac{11}{5} \bar{q}_k - \frac{\boldsymbol{1}}{\boldsymbol{2}} \bar{\boldsymbol{m}}_{\boldsymbol{nnk}} \right], \tag{15b}$$

$$q_n = -\sqrt{\frac{2}{\pi}} \frac{\chi}{2-\chi} \left[2\mathcal{T} + \frac{1}{2} \sigma_{nn} + \frac{5}{28} R_{nn} + \frac{\Delta}{15} \right], \tag{15c}$$

$$m_{nnn} = \sqrt{\frac{2}{\pi}} \frac{\chi}{2-\chi} \left[\frac{2}{5} \mathcal{T} - \frac{7}{5} \sigma_{nn} - \frac{1}{14} R_{nn} + \frac{\Delta}{75} \right], \tag{15d}$$

$$\tilde{m}_{nij} = -\sqrt{\frac{2}{\pi}}\frac{\chi}{2-\chi}\left[\widetilde{\sigma}_{ij} + \frac{1}{14}\widetilde{R}_{ij}\right]. \tag{15e}$$

A comparison of PBC (12) with MBC (15), derived for the Maxwell's accommodation model, allows us to identify

$$\begin{aligned} &\varsigma_0 = \sqrt{\frac{2}{\pi}}\frac{\chi}{2-\chi}, \quad \tau_0 = \sqrt{\frac{2}{\pi}}\frac{2\chi}{2-\chi}, \\ &\varsigma_1 = \varsigma_0, \qquad \varsigma_2 = 13\varsigma_0, \qquad \tau_1 = \frac{\tau_0}{5}, \quad \tau_2 = \frac{26\tau_0}{25}, \quad \tau_3 = \tau_0. \end{aligned} \tag{16}$$

With the coefficients given in (16) and the Burnett coefficients from Table I, the difference between the PBC from Equations (12) and the MBC for the Maxwell's accommodation model is in the underlined terms of Eqs. (12) and (15). We shall show in the next example that macroscopic boundary conditions (15) lead to the violation of the Onsager reciprocity relation,[33–35,50] whereas the phenomenological boundary conditions satisfy the Onsager reciprocity relation for all Knudsen numbers.

B. An example: Rarefied gas flow in a long capillary

We consider a gas flow between two reservoirs, joined by a circular capillary of radius r_0 and length $L\,(\gg r_0)$, as depicted in Fig. 1. The flow is driven by either a constant pressure gradient, $\mathcal{P} = \partial p/\partial z$, in z-direction, while the temperature in both reservoirs is the same (i.e., pressure driven Poiseuille flow) or a constant temperature gradient, $\tau = \partial T/\partial z$, along z-direction, while the pressure in both reservoirs is the same (i.e., transpiration flow).

A cylindrical coordinate system $x_i = \{r, \phi, z\}$ is most appropriate for this problem, where r, ϕ, and z are the radial, azimuthal, and axial coordinates, respectively. The flow is assumed to be fully developed, in steady state, axisymmetric and $v_i = \{0, 0, v_z\}$. The solution of the linear R13 equations, under these assumptions, is obtained as[50]

$$\sigma_{rz} = -\mathcal{P}\frac{r}{2}, \qquad v_z = \mathsf{c}_1 + \mathcal{P}\frac{r^2}{4\mathrm{Kn}} - \frac{\mathrm{Pr}\,\varpi_3}{5}q_z, \tag{17a}$$

$$q_z = \mathcal{P}\frac{\mathrm{Kn}\theta_4}{2} - \tau\frac{5\mathrm{Kn}}{2\,\mathrm{Pr}} + \mathsf{c}_2\mathcal{I}_0\left(\frac{\beta}{\mathrm{Kn}}r\right), \tag{17b}$$

$$R_{rz} = -\frac{5\mathsf{c}_2}{\mathrm{Pr}\,\beta\theta_2}\mathcal{I}_1\left(\frac{\beta}{\mathrm{Kn}}r\right) \text{ and } m_{rrz} = \mathcal{P}\frac{3\mathrm{Kn}}{5\mathrm{Pr_M}}, \tag{17c}$$

where $\mathcal{I}_0$ and $\mathcal{I}_1$ are the modified Bessel functions of the first kind and $\beta = 5\sqrt{\frac{\mathrm{Pr_R}}{14\,\mathrm{Pr}\,\theta_2}}$. The integrating constants, c_1 and c_2, are obtained from boundary conditions (12) or (15).

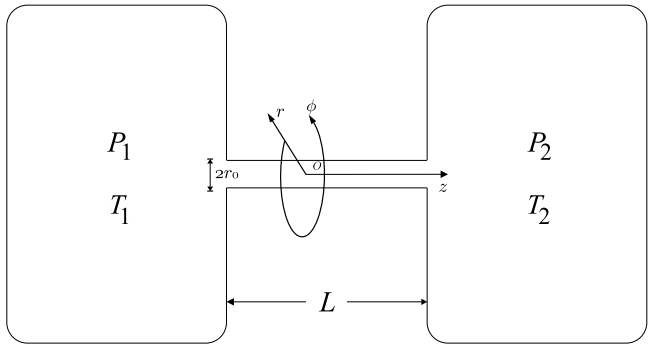

FIG. 1. Schematic diagram illustrating Poiseuille flow and thermal transpiration flow through a long capillary.

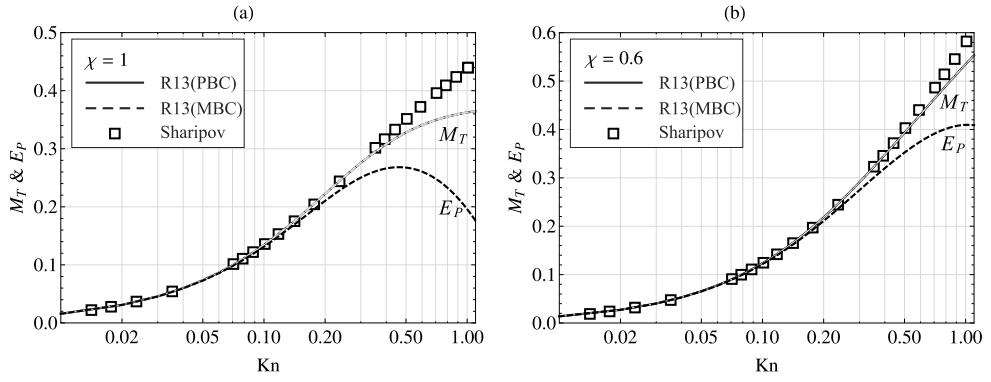

FIG. 2. Validity of Onsager-Casimir reciprocity relation ($E_P = M_T$) in long tube: Reduced thermal energy flow rate (E_P) in Poiseuille flow and the reduced mass flow rate (M_T) in transpiration flow are compared for the phenomenological boundary conditions (solid lines) and macroscopic boundary conditions (dashed lines) applied to the R13 equations with the Maxwell molecules collision model. The results of the R13 equations for $\chi = 1.0$ and 0.8 are compared to the solution of the linearized Boltzmann equation (symbols) from Ref. 35, over moderate Knudsen numbers. Note that the R13 equations with PBC give $E_P = M_T$ for all Knudsen numbers. Also the curves for E_P and M_T as predicted with the phenomenological boundary conditions coincide with M_T predicted with the macroscopic boundary conditions, for all Knudsen numbers. On the other hand, the macroscopic boundary conditions yield $E_P \simeq M_T$ only for Kn $\lesssim 0.25$.

The quantities of interest are the reduced thermal energy flow rate in the Poiseuille flow, E_P, and the reduced mass flow rate in transpiration flow, M_T, defined as in Refs. 35 and 50, i.e.,

$$E_P = \frac{4}{\sqrt{2}} \int_0^1 q_z r dr, M_T = \frac{4}{\sqrt{2}} \int_0^1 v_z r dr. \tag{18}$$

For the steady state flow in the linear regime, Sharipov[33–35] derived the Onsager-Casimir reciprocity relations as $E_P = M_T$ for the entire range of Knudsen numbers. In Fig. 2, E_P and M_T are compared for the PBC and MBC using the R13 equations. The results of the R13 equations with Maxwell molecules collision model are shown in Figs. 2(a) and 2(b) for $\chi = 1$ and 0.6, respectively. The solution of the Boltzmann equation for the reduced mass flow rate, obtained in Ref. 35, is also given in Fig. 2 for a comparison.

As shown in Fig. 2, the phenomenological boundary conditions and macroscopic boundary conditions both give the same reduced mass flow rate in transpiration flows. Furthermore, the phenomenological boundary conditions obey the reciprocity relation ($E_p = M_T$) for all Knudsen numbers; on the other hand, the macroscopic boundary conditions predict $E_p \simeq M_T$ only for Kn $\lesssim 0.25$. However, not surprisingly, they both differ from Boltzmann results at larger Knudsen numbers. Here, it should be clearly stated that the Prandtl number given by the S-model and Maxwell molecules is the same; however, they differ in other Burnett coefficients. Therefore, the comparison between the S-model and Maxwell molecules is more qualitative rather than quantitative.

To summarize, macroscopic boundary conditions for the Maxwell's accommodation model, derived using Grad's closure, may violate the reciprocity relation for high Knudsen numbers, whereas phenomenological boundary conditions satisfy the reciprocity relation for all models as long as the matrix ς in Eq. (13) is positive definite. This poor behavior of macroscopic boundary conditions stems from the approximation $f \simeq f_{|26}^{\text{Grad}}$ near the boundary in the derivation of MBC. Nevertheless, macroscopic boundary conditions provide an approximation for the phenomenological coefficients in phenomenological boundary conditions through Eqs. (16). For convenience, we shall write $\varsigma_i = \frac{\chi}{2-\chi}\sqrt{\frac{2}{\pi}}\varsigma_i^*$ and $\tau_i = \frac{2\chi}{2-\chi}\sqrt{\frac{2}{\pi}}\tau_i^*$, where ς_i^* and τ_i^* are correction coefficients with first approximations (16) as $\varsigma_i^* \simeq \tau_i^* \simeq 1$.

V. CORRECTIONS FOR THE PHENOMENOLOGICAL COEFFICIENTS ς_i^* AND τ_i^*

In what follows next, due to the considered geometries, the underlined terms in PBC (15) and MBC (15) vanish, and therefore the PBC and MBC both agree for $\varsigma_i^* = \tau_i^* = 1$. In this section,

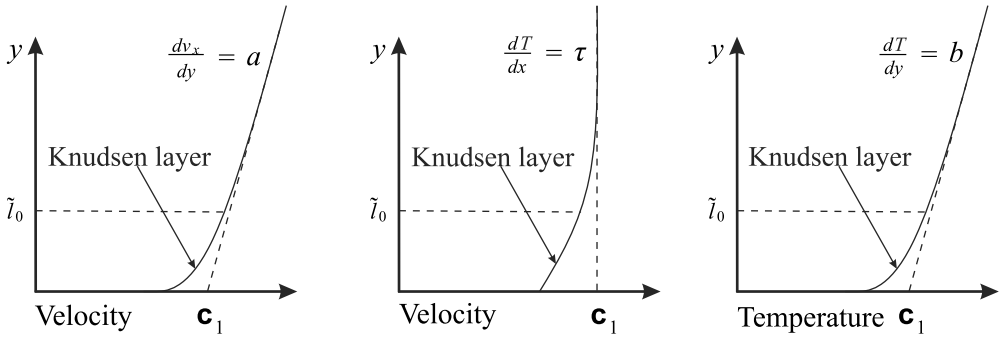

FIG. 3. Schematic diagrams illustrating (a) viscous flow, (b) transpiration flow, and (c) temperature jump.

we shall investigate the effect of ς_i^* and τ_i^* on the slip and jump coefficients and match them with those obtained from the linearized Boltzmann solutions for viscous slip and thermal creep and temperature jump problems.[23,24,28]

For viscous slip and thermal creep problems, the coordinates are chosen such that the wall is parallel to the x-direction and y is the direction perpendicular to the wall which is located at $y = 0$. The wall is stationary and kept at an ambient temperature T_0. Flow is assumed to be in steady-state, where velocity, temperature, and all other flow parameters will depend only on the y-coordinate and the only non-zero velocity component is along the x-direction.

In the viscous slip problem, also known as Kramers' problem, the asymptotic velocity is assumed to be a linear function of y, and there is a constant velocity gradient normal to the wall in the y-direction, i.e., $\lim_{y\longrightarrow\infty} dv_x/dy = a$, see Fig. 3(a). In thermal transpiration flow, $\lim_{y\longrightarrow\infty} dv_x/dy = 0$ and the flow is driven by a constant temperature gradient in x-direction, i.e., $\partial T/\partial x = \tau$, while the pressure gradient along the flow direction is zero, see Fig. 3(b). The temperature jump problem in Fig. 3(c) will be discussed in Sec. V D.

In Ref. 28, Ohwada *et al.* computed the viscous slip and thermal creep coefficients by solving the linearized Boltzmann equation for the viscous slip and thermal creep flow problems, with the fully diffusive (i.e., $\chi = 1$) boundary conditions. Siewert and Sharipov[36] applied the discrete-ordinates method to various model equations to obtain the viscous-slip and the thermal-slip coefficients for both the Maxwell boundary condition and the Cercignani–Lampis boundary condition.

A. Solution of linearized R13 equations

The equations involved in the viscous slip and transpiration flow problems, from the linearized R13 moment system of Equations (2)–(4), reduce to

$$\frac{d\sigma_{xy}}{dy} = 0, \frac{dv_x}{dy} + \frac{\Pr\varpi_3}{5}\frac{dq_x}{dy} = -\frac{\sigma_{xy}}{\mathrm{Kn}}, \frac{5}{2\Pr}\tau + \frac{\Pr\theta_2}{5}\frac{dR_{xy}}{dy} = -\frac{q_x}{\mathrm{Kn}}. \tag{19}$$

The R13 constitutive relations, obtained from Equations (4), are

$$m_{xyy} = 0, R_{xy} = -\frac{14}{5}\frac{\mathrm{Kn}}{\mathrm{Pr_R}}\frac{dq_x}{dy}. \tag{20}$$

The general solution for Equations (19) and (20) reads

$$\sigma_{xy} = -a\mathrm{Kn}, v_x = \mathbf{c}_1 + ya - \frac{\Pr\varpi_3}{5}\left(\mathbf{c}_2 e^{-\frac{y\beta}{\mathrm{Kn}}} + \mathbf{c}_3 e^{\frac{y\beta}{\mathrm{Kn}}}\right), \tag{21a}$$

$$q_x = -\frac{5\mathrm{Kn}}{2\Pr}\tau + \left(\mathbf{c}_2 e^{-\frac{y\beta}{\mathrm{Kn}}} + \mathbf{c}_3 e^{\frac{y\beta}{\mathrm{Kn}}}\right), \tag{21b}$$

$$R_{xy} = \frac{14\beta}{5\mathrm{Pr_R}}\left(\mathbf{c}_2 e^{-\frac{y\beta}{\mathrm{Kn}}} - \mathbf{c}_3 e^{\frac{y\beta}{\mathrm{Kn}}}\right), m_{xyy} = 0, \tag{21c}$$

where $\mathbf{c}_1$, $\mathbf{c}_2$, $\mathbf{c}_3$ are constants of integration. In the above solutions, as $y \to \infty$, q_x and R_{xy} must remain finite; therefore, $\mathbf{c}_3 = 0$. For both flow configurations, integration constants, $\mathbf{c}_1$, $\mathbf{c}_2$ in Eqs. (21), are evaluated from boundary conditions (12a) and (12b). They are presented in Appendix B 1. To be consistent with the dimensionless kinetic solutions given in Refs. 28 and 36, we took $L_0 = \tilde{l}_0\sqrt{\pi}/2$ and $\mathrm{Kn} = \tilde{\mu}/\sqrt{2}$, where $\tilde{l}_0$ and $\tilde{\mu}$ are mean free path and dimensionless viscosity ($\tilde{\mu} = 1$ for BGK and $\tilde{\mu} = 1.27$ for hard sphere[28]).

B. Results for viscous-slip and thermal creep coefficients

The viscous-slip coefficients η_{VS} and thermal creep coefficients η_{TC}, defined as

$$\eta_{\mathrm{VS}} = \frac{\chi}{2-\chi}\frac{\mathbf{c}_1}{a\mathrm{Kn}\sqrt{\frac{\pi}{2}}}, \eta_{\mathrm{TC}} = \frac{\chi}{2-\chi}\frac{\mathbf{c}_1}{\tau\mathrm{Kn}}, \tag{22}$$

are compared with the linearized Boltzmann solutions. The viscous-slip coefficients for $\chi = 1$ are listed in Table III. From Table III, η_{VS} as predicted from macroscopic boundary conditions (i.e., $\varsigma_i^* = 1$) are about 10%, 6%, and 8% smaller than the reference values obtained from the linearized Boltzmann equation with BGK,[28] HS,[28] and MMs collision models,[23] respectively. The values of the thermal creep coefficient, $\eta_{,\mathrm{TC}}$ are also listed in Table III, together with the reference solutions for the linearized Boltzmann equation with BGK and hard sphere collision models. We could not find any data for thermal creep with the Maxwell molecules collision model. For BGK and hard sphere collision models, the macroscopic boundary conditions predictions are about 6% and 16% smaller than the reference solutions, respectively.

Viscous slip and thermal creep coefficients strongly depend on ς_0^* and ς_1^* through $\mathbf{c}_1$ given in Appendix B 1, and only weakly depend on ς_2^*; hence, we choose $\varsigma_2^* = 1$ (the value given by the Maxwell accommodation model). Furthermore, the values for $\varsigma_{0,1}^*$ can be chosen accordingly to give proper viscous slip coefficient, η_{VS} and thermal creep coefficient η_{TC}. The corresponding values for the phenomenological coefficients ς_0^* and ς_1^*, are given in Table III.

C. Detailed flow profiles for viscous slip and thermal creep flows

The profiles of defect velocity, $v_x - ay$, for the viscous slip problem are shown in Fig. 4(a). The R13 solutions from Eqs. (21) obtained using macroscopic boundary conditions (dashed curve) and phenomenological boundary conditions (solid curve) with correction coefficients given from Table III are shown and compared with the results of the linearized Boltzmann equation with hard sphere collision model[28] (circles). For proper scaling, the kinetic data are multiplied with the factor $\sqrt{2}$.

TABLE III. Viscous-slip coefficients η_{VS} and thermal creep coefficients η_{TC} for BGK, hard sphere (HS), and the Maxwell molecules (MMs) collision models. Results obtained from the R13 equations with MBC are compared with the linearized Boltzmann equation (LBE) with BGK,[28] hard sphere (HS),[28] and Maxwell molecules (MM)[23] collision models. Corresponding values for correction coefficients, ς_i^* are tabulated.

	η_{VS}		η_{TC}				
	MBC	LBE	MBC	LBE	ς_0^*	ς_1^*	ς_2^*
BGK	1.0373	1.1467[28]	0.7236	0.7663[28]	0.8931	0.7649	1
HS	1.0450	1.1141[28]	0.8572	1.0178[28]	0.9088	0.5118	1
MM	1.0431	1.1366[23]	1.1378	...	0.9143	0.9143	1

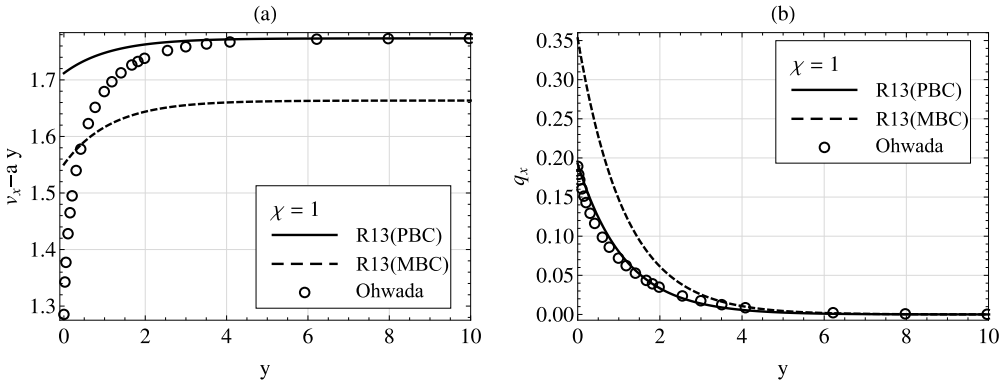

FIG. 4. (a) Defect velocity and (b) tangential heat flux for the viscous slip problem: the R13 solutions obtained using macroscopic boundary conditions (denoted by dashed curve) and phenomenological boundary conditions (denoted by solid curve) with correction coefficients. The solution of the linearized Boltzmann equation with hard sphere collision model[28] is denoted by circles.

Clearly, the R13 equations are unable to provide an accurate description of the Knudsen layer for velocity. From Eqs. (21), the R13 equations provide only one exponential function to describe the velocity in the Knudsen layer. The moment method approach, however, approximates the Knudsen layer as superposition of many exponential functions;[43] hence, to fully resolve Knudsen layers, a sufficiently large number of moment equations are required. For example, the R26 equations provide two exponential layers to describe the velocity close to the wall, which provides a significant improvement in describing Knudsen layers.[17] However, the convergence and uniqueness of the moment equations to the solution of the Boltzmann equations is not entirely clear. Torrilhon in Ref. 54 studies the convergence of moment hierarchies. For the cases studied in Ref. 54, the results show an initial non-monotonic convergence behavior for the considered families of moment equations but all systems of equations resolve Knudsen layers eventually when a sufficiently large number of moments are included.

Here, we are interested in the bulk behavior, in which the magnitude of the defect velocity given from Eq. (B1) is inversely proportional to ς_0^*. The macroscopic boundary conditions give $\varsigma_0^* = 1$; hence, in comparison to the linearized Boltzmann equation where $\varsigma_0^* \simeq 0.9$, the macroscopic boundary conditions underpredict the defect velocity. As shown in Figure 4(a), the phenomenological boundary conditions give an accurate description of the bulk behavior, with the coefficients ς_i^* and τ_i^* given the Table III. The profiles for tangential heat flux are shown in Fig. 4(b). In the viscous slip problem, tangential heat flux is a rarefaction effect due to Knudsen layers, which cannot be predicted by NSF. The magnitude of tangential heat flux is proportional to the ratio $\varsigma_1^*/\varsigma_0^*$, given from Eq. (B6). The macroscopic boundary conditions give $\varsigma_1^*/\varsigma_0^* = 1$, whereas from Table III, this value is about 0.56; hence, the R13 equations, with macroscopic boundary conditions, overpredict the heat flux, while the phenomenological boundary conditions with corrected coefficients from Table III provide a good match.

In Fig. 5, profiles of velocity and heat flux in transpiration flow are shown for $\chi = 1$, with hard sphere collision model. Plots (a) and (b) compare the velocity and heat flux solutions of R13 equations, respectively, using macroscopic boundary conditions and phenomenological boundary conditions and linear Boltzmann equation solutions. The solution of the R13 equations with macroscopic boundary conditions shows about 15% error in transpiration velocity, with respect to kinetic data in the bulk. This error is corrected by using phenomenological boundary conditions with the coefficients provided in Table III. Note that, in transpiration flow, the magnitude of tangential heat flux only mildly depends on ς_i^* through $\mathbf{c}_0$ in Eq. (B4). Therefore, in this case, the macroscopic boundary conditions and phenomenological boundary conditions both give similar solutions for the tangential heat flux. The results presented so far were exclusively for $\chi = 1$. In Ref. 36, Siewert solved the Boltzmann equation—for fully diffusive to specular walls—to determine the velocity slip and thermal creep coefficients, which we used to establish the relationship between

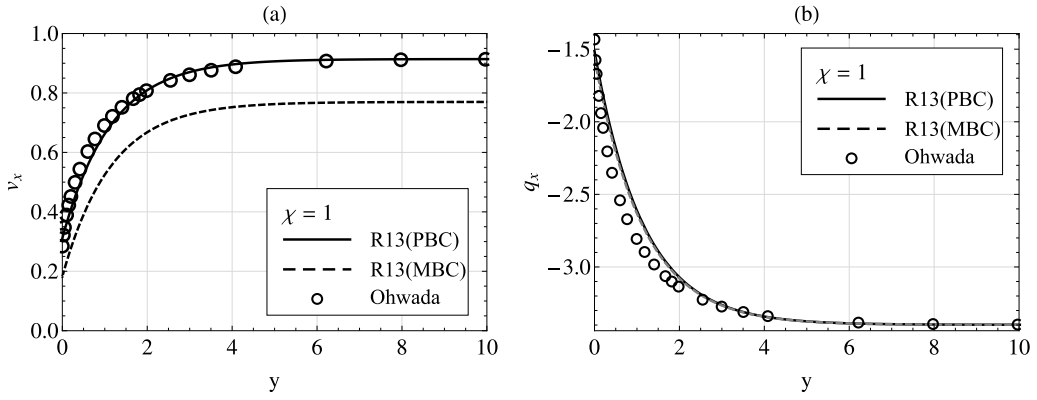

FIG. 5. (a) Defect velocity and (b) tangential heat flux for the transpiration flow problem: the R13 solutions obtained using macroscopic boundary conditions (denoted by dashed curve) and phenomenological boundary conditions (denoted by solid curve) with correction coefficients. The solution of the linearized Boltzmann equation with hard sphere collision model[28] is denoted by circles.

phenomenological coefficients ς_i^* and accommodation coefficient χ. In Fig. 6, we show (a) the slip coefficient $\eta_{\rm VS}$ and (b) transpiration coefficient $\eta_{\rm TC}$ versus accommodation coefficient χ, using $\varsigma_0^* = 0.9952 - 0.1033\chi$, $\varsigma_1^* = 0.9853 - 0.2241\chi$, and $\varsigma_2^* = 1$ for BGK, $\varsigma_0^* = 0.9949 - 0.0874\chi$, $\varsigma_1^* = 0.5587 - 0.047\,98\chi$, and $\varsigma_2^* = 1$ for hard sphere, and $\varsigma_0^* = \varsigma_1^* = 0.9985 - 0.085\chi$ and $\varsigma_2^* = 1$ for Maxwell molecules collision models. These expressions for ς_i^* are obtained by linear fitting with kinetic data from Refs. 36 and 56 for the BGK and hard sphere collision models, respectively, and Ref. 23 for the Maxwell molecules collision model.

D. Temperature jump problem

In the temperature jump problem, one considers stationary heat transfer in a gas occupying the $y \geq 0$ half-space domain with one wall located at $y = 0$, as demonstrated in Fig. 3(c). Far from the wall, the temperature is a linear function and there is a constant temperature gradient in y-direction, i.e., $\lim_{y\longrightarrow\infty} dT/dy = b$. The equations involved in the temperature jump problem are obtained from

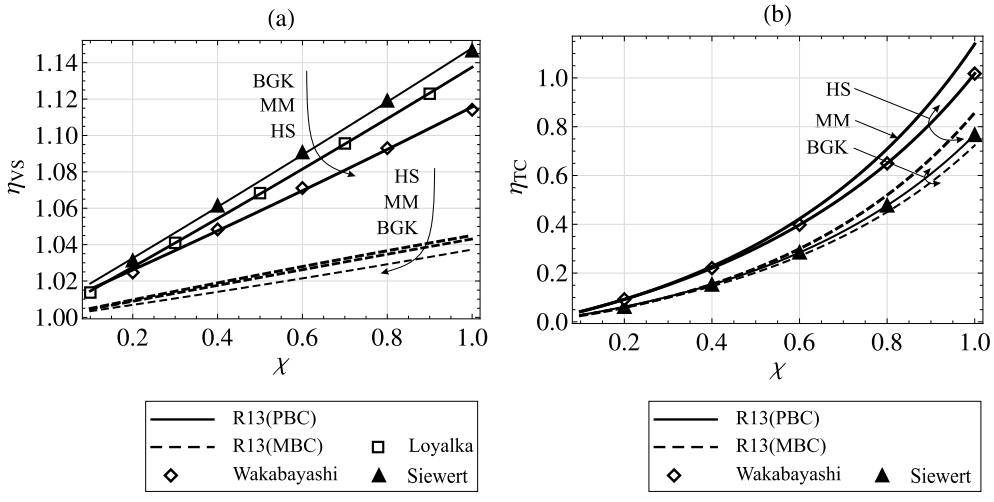

FIG. 6. (a) Viscous slip coefficients, $\eta_{,\rm VS}$ and (b) thermal creep coefficients, $\eta_{\rm TC}$, are plotted with respect to the accommodation coefficient χ. Results obtained form the linearized R13 equations with phenomenological boundary conditions (continuous line) and macroscopic boundary conditions (dashed lines) are compared with the reference solutions of linearized Boltzmann equation with BGK,[36] hard sphere,[56] and Maxwell molecules[23] collision models (denoted by symbols).

TABLE IV. Temperature jump coefficient η_{TJ} for BGK,[39] hard sphere,[39] and the Maxwell molecules[22] collision models are compared between the R13 equations using MBC and linearized Boltzmann equations. Corresponding values for correction coefficients, τ_i^*, are tabulated.

	η_{TJ}				
	MBC	LBE	τ_0^*	τ_1^*	τ_2^*
BGK	1.0189	1.1760[39]	0.8642	0.8642	1
HS	1.0207	1.1267[39]	0.9041	0.9041	1
MM	1.0209	1.1621[22]	0.8762	0.8762	1

Equations (2c), (3a), and (3b) as

$$\frac{dq_y}{dy} = 0, \frac{\theta_4}{2}\frac{d\sigma_{yy}}{dy} + \frac{5}{2\,\mathrm{Pr}}\frac{dT}{dy} = -\frac{q_y}{\mathrm{Kn}}, \frac{\varpi_2}{2}\frac{dm_{yyy}}{dy} = -\frac{\sigma_{yy}}{\mathrm{Kn}}. \tag{23}$$

The R13 constitutive relationships, obtained from Equations (4), are

$$m_{yyy} = -\frac{9\mathrm{Kn}}{5\mathrm{Pr_M}}\frac{d\sigma_{yy}}{dy}, R_{yy} = 0, \text{ and } \Delta = 0. \tag{24}$$

The solution obtained from the Eqs. (23) and (24) is

$$q_y = -\frac{5\mathrm{Kn}}{2\,\mathrm{Pr}}b, T = \mathbf{c}_1 + yb - \frac{\mathrm{Pr}\,\theta_4}{5}\left(\mathbf{c}_2 e^{-\frac{y\gamma}{\mathrm{Kn}}} + \mathbf{c}_3 e^{\frac{y\gamma}{\mathrm{Kn}}}\right),$$
$$\sigma_{yy} = \mathbf{c}_2 e^{-\frac{y\gamma}{\mathrm{Kn}}} + \mathbf{c}_3 e^{\frac{y\gamma}{\mathrm{Kn}}}, m_{yyy} = \frac{9\gamma}{5\mathrm{Pr_M}}\left(\mathbf{c}_2 e^{-\frac{y\gamma}{\mathrm{Kn}}} - \mathbf{c}_3 e^{\frac{y\gamma}{\mathrm{Kn}}}\right),$$

where $\gamma = \sqrt{\frac{10\mathrm{Pr_M}}{9\varpi_2}}$, and $\mathbf{c}_1$, $\mathbf{c}_2$, $\mathbf{c}_3$ are constants of integration, with $\mathbf{c}_3 = 0$, because, as $y \to \infty$, σ_{yy} and m_{yyy} must remain finite. The remaining constants $\mathbf{c}_1$, $\mathbf{c}_2$, obtained from boundary conditions (12c) and (12d), are given in Appendix B 2. The temperature jump coefficient, η_{TJ}, defined as

$$\eta_{\mathrm{TJ}} = \frac{4\,\mathrm{Pr}}{5}\sqrt{\frac{2}{\pi}}\frac{\chi}{2-\chi}\frac{\mathbf{c}_1}{b\,\mathrm{Kn}}, \tag{25}$$

for $\chi = 1$, is listed in Table IV. As with the case of viscous slip and thermal creep, the R13 equations with macroscopic boundary conditions underpredict the temperature jump coefficient by

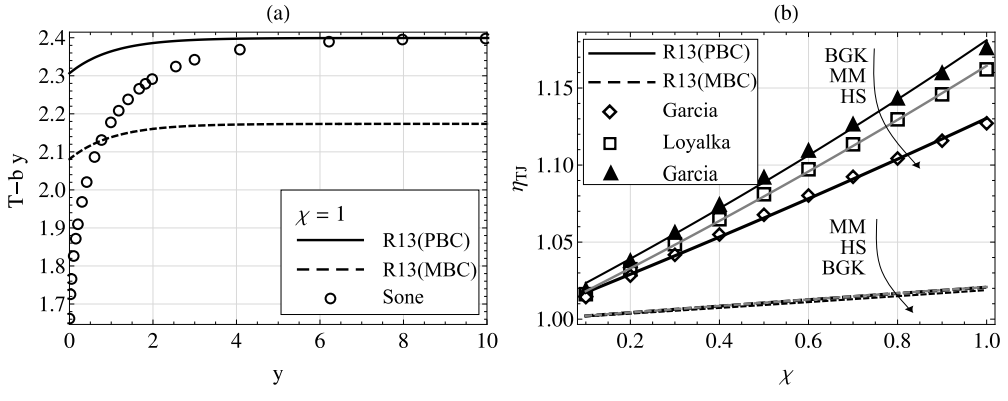

FIG. 7. (a) R13 solutions with phenomenological boundary conditions (solid curves) and macroscopic boundary conditions (dashed curves) for the temperature defect comparing with the linearized Boltzmann solutions for hard sphere collision model (denoted by circles), Ref. 39 with fully diffusive wall and Kn = 0.8980. (b) Comparison of temperature jump coefficient η_{TJ} obtained from the R13 equations with macroscopic boundary conditions and the phenomenological boundary conditions with those obtained from the linearized Boltzmann equation for BGK and hard sphere from Ref. 12 and Maxwell molecules Ref. 22 collision model.

about 13%, 9%, and 12% with respect to the linear Boltzmann equation with BGK,[39] hard sphere,[39] and Maxwell molecules[22] collision models, respectively. The corresponding correction coefficients, τ_i^*, are also listed in Table IV. Figure 7(a) presents the R13 solutions for the temperature defect, $T - by$, in comparison to the Boltzmann solutions for the hard sphere collision model.[39] Results are presented with fully diffusive walls ($\chi = 1$), and $b = 1$ with Kn = 0.8980 $\left(=\tilde{\mu}/\sqrt{2}\right)$. In Fig. 7(a), as before, the R13 equations cannot capture the Knudsen layer profile for temperature. Here, as well as in the earlier case, the offset in the bulk value results from the mismatch in the temperature jump and Knudsen layer at the boundary. With PBC corrections, the overall jump is corrected such that the bulk value is rectified. The results for the temperature jump coefficient η_{TJ} are shown in Fig. 7(b). Here, we compare the temperature jump coefficient obtained from the Boltzmann equation with those obtained from the R13 equations with macroscopic boundary conditions (i.e., $\tau_i^* = 1$) and the phenomenological boundary conditions with correction factors $\tau_0^* = \tau_1^* = 0.9920 - 0.1315\chi$, $\tau_2^* = 1$ for BGK, $\tau_0^* = \tau_1^* = 0.9944 - 0.0932\chi$, $\tau_2^* = 1$ for hard sphere, and $\tau_0^* = \tau_1^* = 0.9965 - 0.1221\chi$, $\tau_2^* = 1$ for Maxwell molecules collision model. These expressions for τ_i^* are obtained by linear fitting to match the temperature jump coefficients for the linearized Boltzmann equation for BGK and hard sphere from Ref. 12 and Maxwell molecules Ref. 22 collision model.

VI. CONCLUSION

Evidently, the R13 equations cannot describe Knudsen layers completely due to the lack of sublayer contributions from higher moments. Knudsen layers arise from an eigenvalue problem for the moment equations, and thus to fully capture the Knudsen layer one must consider moment equations much beyond the 13 moments. Note that the moment equations themselves are not derived for the bulk flow, but from the Boltzmann equation, without any statement of being close or away from the wall. So the moment equations able to approximate the Knudsen-layer dominated processes accurately provided a sufficient number of moments which are considered in the approximation, although convergence is not proven. The question remains how to obtain an accurate result with as few moment variables as possible.

This paper presented a phenomenological approach to the boundary conditions for the linearized R13 equations using the second law of thermodynamics. To generalize earlier work,[45] in this paper, we considered the cross-coupling between terms of the same tensorial structure. This procedure allowed us to identify and estimate the values of the unknown coefficients appearing in these phenomenological boundary conditions. It was also shown that the macroscopic boundary conditions, derived using Grad's closure, violate the reciprocity relation for high Knudsen numbers, whereas the phenomenological boundary conditions satisfy the reciprocity relation for all Knudsen numbers and collision models, although the R13 equations are only accurate for small Knudsen numbers. The classical half-space problems of velocity slip, thermal creep, and temperature jump problems were revisited using the R13 equations. The macroscopic boundary conditions underpredict the slip, jump, and creep coefficients. The presented approach allowed us to systematically correct this mismatch through phenomenological coefficients, which were determined by comparing the R13 solutions with the linearized Boltzmann equations for three collision models (BGK, hard sphere, and Maxwell molecules) for arbitrary accommodation coefficient.

ACKNOWLEDGMENTS

This work was supported by the National Research Foundation of Korea funded by the Ministry of Education, Science and Technology (Basic Science Research Program No. NRF 2012-046270), Republic of Korea.

APPENDIX A: NORMAL AND TANGENTIAL COMPONENTS OF VECTORS AND TENSORS

The normal and tangential components of a vector q_i are defined as

$$q_n = q_k n_k \text{ and } \bar{q}_i = q_i - q_n n_i, \tag{A1}$$

respectively, and therefore by definition $\bar{q}_k n_k = 0$. Similarly, for a second order tensor σ_{ij} (trace free and symmetric), we can define a normal-normal component, σ_{nn}, normal-tangential vector, $\bar{\sigma}_{ni}$, and tangential-tangential tensor, $\widetilde{\sigma}_{ij}$, as

$$\sigma_{nn} = \sigma_{rk} n_k n_r, \tag{A2a}$$

$$\bar{\sigma}_{ni} = \sigma_{ik} n_k - \sigma_{nn} n_i, \tag{A2b}$$

$$\widetilde{\sigma}_{ij} = \sigma_{ij} - \sigma_{nn}\left(\frac{3}{2} n_i n_j - \frac{1}{2}\delta_{ij}\right) - \bar{\sigma}_{ni} n_j - \bar{\sigma}_{nj} n_i, \tag{A2c}$$

where by definition $\bar{\sigma}_{nk} n_k = 0 = \widetilde{\sigma}_{kk}$ and $\widetilde{\sigma}_{ik} n_k = 0$. For a third order tensor m_{ijk} (symmetric and trace free), we may define

$$m_{nnn} = m_{ijk} n_i n_j n_k, \tag{A3a}$$

$$\bar{m}_{nni} = m_{ijk} n_j n_k - m_{nnn} n_i, \tag{A3b}$$

$$\widetilde{m}_{nij} = m_{ijk} n_k - m_{nnn}\left(\frac{3}{2} n_i n_j - \frac{1}{2}\delta_{ij}\right) - \bar{m}_{nni} n_j - \bar{m}_{nnj} n_i. \tag{A3c}$$

Hence, by definition, $\bar{m}_{nnk} n_k = 0$, $\widetilde{m}_{nik} n_k = 0$, and $\widetilde{m}_{nkk} = 0$.

APPENDIX B: INTEGRATION CONSTANTS

1. Viscous slip and thermal creep problems

Integrating constants obtained from Equations (12a) and (12b), for the viscous slip problem, simplify to

$$\mathbf{c}_1 = \sqrt{\frac{\pi}{2}} a\mathrm{Kn}\left(\frac{1}{\varsigma_0^* \alpha^*} + \frac{\varsigma_1^{*2}}{\varsigma_0^{*2}} \frac{2\theta_2 \mathrm{Pr}^2 \mathrm{Pr_R}}{\mathbf{c}_0}\right), \tag{B1}$$

$$\mathbf{c}_2 = \sqrt{\frac{\pi}{2}} a\mathrm{Kn}\left(\frac{\varsigma_1^*}{\varsigma_0^*} \frac{25\mathrm{Pr_R}}{\mathbf{c}_0}\right), \tag{B2}$$

and for the thermal creep problem, they read

$$\mathbf{c}_1 = \tau\mathrm{Kn}\left(\frac{\varpi_3}{2} - \frac{\varsigma_1^*}{\varsigma_0^*} \frac{5\sqrt{7\pi\theta_2 \mathrm{Pr}\,\mathrm{Pr_R}}}{\mathbf{c}_0}\right), \tag{B3}$$

$$\mathbf{c}_2 = \frac{5}{2\,\mathrm{Pr}}\tau\mathrm{Kn}\left(1 - \frac{25}{\mathrm{Pr}\,\theta_2} \frac{\sqrt{7\pi\theta_2 \mathrm{Pr}\,\mathrm{Pr_R}}}{\mathbf{c}_0}\right), \tag{B4}$$

where we used abbreviations $\mathbf{c}_0 = \frac{25}{\mathrm{Pr}\,\theta_2}\sqrt{7\pi\theta_2 \mathrm{Pr}\,\mathrm{Pr_R}} + 2\theta_2 \mathrm{Pr}^2 \mathrm{Pr_R} \varsigma_0^* \alpha^* \left(13\frac{\varsigma_2^*}{\varsigma_0^*} - \frac{\varsigma_1^{*2}}{\varsigma_0^{*2}}\right)$ and $\alpha^* = \frac{\chi}{2-\chi}$.

2. Temperature jump problem

Similarly, the constants for temperature jump problem can be obtained from their boundary conditions (12c) and (12d) as

$$\mathbf{c}_1 = \frac{5}{4\,\mathrm{Pr}}\sqrt{\frac{\pi}{2}} b\mathrm{Kn}\left(\frac{1}{\alpha^* \tau_0^*} + \frac{\tau_1^{*2}}{\tau_0^{*2}} \frac{\mathrm{Pr_M}}{\mathbf{c}_0}\right), \tag{B5}$$

$$\mathbf{c}_2 = \frac{5}{4\,\mathrm{Pr}}\sqrt{\frac{\pi}{2}} b\mathrm{Kn}\left(\frac{\tau_1^*}{\tau_0^*} \frac{40\mathrm{Pr_M}}{3\varpi_2 \mathbf{c}_0}\right), \tag{B6}$$

where $\mathbf{c}_0 = \frac{10}{\varpi_2}\sqrt{\frac{20\pi \mathrm{Pr_M}}{\varpi_2}} + \mathrm{Pr_M} \tau_0^* \alpha^* \left(26\frac{\tau_2^*}{\tau_0^*} - \frac{\tau_1^{*2}}{\tau_0^{*2}}\right)$ and $\alpha^* = \frac{\chi}{2-\chi}$.

APPENDIX C: DETAILS REGARDING THE DERIVATION OF PHENOMENOLOGICAL BOUNDARY CONDITIONS

The coupling between the cross terms of the same tensorial structure,[21] i.e., scalars (q_n, m_{nnn}), vectors ($\bar{\sigma}_{nk}$, $\bar{R}_{nk}$), and matrix $\widetilde{m}_{nij}$ allows us to write Equation (11) as

$$\Sigma_W^{\mathrm{LR13}} = \sum_{a=0}^{2} \Sigma_a = -\sum_{a=0}^{2} \mathcal{J}_a \cdot \mathcal{F}_a. \tag{C1}$$

Here, Σ_a is the contribution to the entropy production per unit surface area due to the corresponding thermodynamic force ($\mathcal{F}_a$) and flux ($\mathcal{J}_a$) pairs of the same tensorial structure, i.e., $a = 0, 1, 2$ for scalars, vectors, and rank 2 tensors, respectively. Here, we have thermodynamic forces

$$\mathcal{J}_0 = \{q_n, m_{nnn}\}, \mathcal{J}_1 = \{\bar{\sigma}_{ni}, \bar{R}_{ni}\}, \text{ and } \mathcal{J}_2 = \widetilde{m}_{nij} \tag{C2}$$

and fluxes

$$\mathcal{F}_0 = \left\{ \mathcal{T} + \frac{\varpi_3 \mathrm{Pr}}{5}\sigma_{nn} + \frac{2\theta_2 \mathrm{Pr}^2}{25}\left(R_{nn} + \frac{\Delta}{3}\right), \frac{3\tau_1 \varpi_2 \sigma_{nn}}{8} \right\}, \tag{C3a}$$

$$\mathcal{F}_1 = \left\{ \mathcal{V}_i + \frac{\varpi_3}{5}\mathrm{Pr}\,\bar{q}_i + \frac{\varpi_2}{2}\bar{m}_{nni}, \frac{2\theta_2}{25}\mathrm{Pr}^2\,\bar{q}_i \right\}, \tag{C3b}$$

$$\mathcal{F}_2 = \frac{\varpi_2}{4}\widetilde{\sigma}_{ij}. \tag{C3c}$$

The positivity of the entropy production in (C1) is guaranteed if we take

$$\mathcal{J}_0 = -\tau \cdot \mathcal{F}_0 \text{ and } \mathcal{J}_1 = -\varsigma \cdot \mathcal{F}_1,$$

provided the matrices τ and ς are positive definite.

[1] R. K. Agarwal, K. Yun, and R. Balakrishnan, "Beyond Navier-Stokes: Burnett equations for simulation of transitional flows," Phys. Fluids **13**, 3061 (2001).
[2] G. A. Bird, *Molecular Gas Dynamics and the Direct Simulation of Gas Flows* (Oxford University Press, 1998).
[3] A. V. Bobylev, "Instabilities in the Chapman–Enskog expansion and hyperbolic Burnett equations," J. Stat. Phys. **124**, 371 (2006).
[4] A. V. Bobylev, "Generalized Burnett hydrodynamics," J. Stat. Phys. **132**, 569 (2008).
[5] A. V. Bobylev and A. Windfall, "Boltzmann equation and hydrodynamics at the Burnett level," Kinet. Relat. Models **5**, 237 (2012).
[6] C. Cercignani, *Theory and Application of the Boltzmann Equation* (Scottish Academic Press, 1975).
[7] C. Cercignani and M. Lampis, "Kinetic models for gas-surface interactions," Transp. Theory Stat. Phys. **1**, 101 (1971).
[8] S. Chapman and T. G. Cowling, *The Mathematical Theory of Non-Uniform Gases* (Cambridge University Press, 1970).
[9] P. Curie, *Oeuvres de Pierre Curie: Publées par les Soins de la Société Francaise de Physique* (Gauthier-Villars, Peris, 1908).
[10] S. R. de Groot and P. Mazur, *Non-Equilibrium Thermodynamics* (Dover, 1984).
[11] M. Gad–el–Hak, *The MEMS Handbook: Introduction and Fundamentals* (CRC Press, 2005).
[12] R. D. M. Garcia and C. E. Siewert, "Viscous-slip, thermal-slip, and temperature-jump coefficients based on the linearized Boltzmann equation (and five kinetic models) with the Cercignani Lampis boundary condition," Eur. J. Mech., B: Fluids **29**, 181 (2010).
[13] V. Garzo and A. Santos, *Kinetic Theory of Gases in Shear Flows: Nonlinear Transport* (Springer, Netherlands, 2003).
[14] H. Grad, "On the kinetic theory of rarefied gases," Commun. Pure Appl. Math. **2**, 331 (1949).
[15] H. Grad, *Principles of the Kinetic Theory of Gases*, Handbuch der Physik (Springer, Berlin, 1958), Vol. 12.
[16] X. Gu and D. R. Emerson, "A computational strategy for the regularized 13 moment equations with enhanced wall-boundary conditions," J. Comput. Phys. **225**, 263 (2007).
[17] X. Gu, D. R. Emerson, and G. Tang, "Analysis of the slip coefficient and defect velocity in the Knudsen layer of a rarefied gas using the linearized moment equations," Phys. Rev. E **81**, 016313 (2010).
[18] V. Gupta and M. Torrilhon, "Higher order moment equations for rarefied gas mixtures," Proc. R. Soc. A **471**(2173), 20140754 (2014).
[19] S. Jin and M. Slemrod, "Regularization of the Burnett equations via relaxation," J. Stat. Phys. **103**, 1009 (2001).
[20] G. M. Karniadakis and A. Beskok, *Micro Flows: Fundamentals and Simulation* (Springer, 2002).
[21] S. Kjelstrup, D. Bedeaux, E. Johannessen, and J. Gross, *Non-Equilibrium Thermodynamics for Engineers* (World Scientific Publishing Company, 2010), (Author).
[22] S. K. Loyalka, "Momentum and temperature slip coefficients with arbitrary accommodation at the surface," J. Chem. Phys. **48**, 5432 (1968).
[23] S. K. Loyalka, "Velocity profile in the Knudsen layer for the Kramer's problem," Phys. Fluids **18**, 1666 (1975).
[24] S. K. Loyalka, "Temperature jump and thermal creep slip: Rigid sphere gas," Phys. Fluids A **1**, 403 (1989).

[25] S. K. Loyalka, N. Petrellis, and T. S. Storvick, "Some exact numerical results for the BGK model: Couette, Poiseuille and thermal creep flow between parallel plates," J. Appl. Math. Phys. (ZAMP) **30**, 514 (1979).
[26] C. Maxwell, "On stress in rarefied gases arising from inequalities of temperature," Philos. Trans. R. Soc. London **170**, 231 (1879).
[27] R. S. Myong, "A full analytical solution for the force-driven compressible Poiseuille gas flow based on a nonlinear coupled constitutive relation," Phys. Fluids **23**, 012002 (2011).
[28] T. Ohwada, Y. Sone, and K. Aoki, "Numerical analysis of the shear and thermal creep flows of a rarefied gas over a plane wall on the basis of the linearized Boltzmann equation for hard-sphere molecules," Phys. Fluids A **1**, 1588 (1989).
[29] B. Rahimi and H. Struchtrup, "Capturing non-equilibrium phenomena in rarefied polyatomic gases: A high-order macroscopic model," Phys. Fluids **26**, 052001 (2014).
[30] A. Rana, A. Mohammadzadeh, and H. Struchtrup, "A numerical study of the heat transfer through a rarefied gas confined in a micro cavity," Continuum Mech. Thermodyn. **27**, 433 (2015).
[31] A. Rana, M. Torrilhon, and H. Struchtrup, "A robust numerical method for the R13 equations of rarefied gas dynamics: Application to lid driven cavity," J. Comput. Phys. **236**, 169 (2012).
[32] A. S. Rana, "Numerical simulation of rarefied gas flow in micro and vacuum devices," Ph.D. thesis, University of Victoria, 2014.
[33] F. Sharipov, "Onsager-Casimir reciprocity relations for open gaseous systems at arbitrary rarefaction. I. General theory for single gas," Physica A **203**, 437 (1994).
[34] F. Sharipov, "Onsager-Casimir reciprocity relations for open gaseous systems at arbitrary rarefaction. II. Application of the theory for single gas," Physica A **203**, 457 (1994).
[35] F. Sharipov and V. Seleznev, "Data on internal rarefied gas flows," J. Phys. Chem. Ref. Data **27**, 657 (1998).
[36] C. E. Siewert and F. Sharipov, "Model equations in rarefied gas dynamics: Viscous-slip and thermal-slip coefficients," Phys. Fluids **14**, 4123 (2002).
[37] L. H. Söderholm, "Hybrid Burnett equations: A new method of stabilizing," Transp. Theory Stat. Phys. **36**, 495 (2007).
[38] Y. Sone, *Kinetic Theory and Fluid Dynamics* (Birkhäuser, 2002).
[39] Y. Sone, T. Ohwada, and K. Aoki, "Temperature jump and Knudsen layer in a rarefied gas over a plane wall: Numerical analysis of the linearized Boltzmann equation for hard sphere molecules," Phys. Fluids A **1**, 363 (1989).
[40] H. Struchtrup, "Stable transport equations for rarefied gases at high orders in the Knudsen number," Phys. Fluids **16**, 3921 (2004).
[41] H. Struchtrup, *Macroscopic Transport Equations for Rarefied Gas Flows: Approximation Methods in Kinetic Theory* (Springer, 2005).
[42] H. Struchtrup, "Scaling and expansion of moment equations in kinetic theory," J. Stat. Phys. **125**, 565 (2006).
[43] H. Struchtrup, "Linear kinetic heat transfer: Moment equations, boundary conditions, and Knudsen layers," Physica A **387**, 1750 (2008).
[44] H. Struchtrup and M. Torrilhon, "Regularization of Grad's 13-moment equations: Derivation and linear analysis," Phys. Fluids **15**, 2668 (2003).
[45] H. Struchtrup and M. Torrilhon, "H theorem, regularization, and boundary conditions for linearized 13-moment equations," Phys. Rev. Lett. **99**, 014502 (2007).
[46] H. Struchtrup and M. Torrilhon, "Higher-order effects in rarefied channel flows," Phys. Rev. E **78**, 046301 (2008).
[47] H. Struchtrup and M. Torrilhon, "Regularized 13 moment equations for hard sphere molecules: Linear bulk equations," Phys. Fluids **25**, 052001 (2013).
[48] P. Taheri, A. S. Rana, H. Struchtrup, and M. Torrilhon, "Macroscopic description of steady and unsteady rarefaction effects in boundary value problems of gas dynamics," Continuum Mech. Thermodyn. **21**, 423 (2009).
[49] P. Taheri and H. Struchtrup, "Effects of rarefaction in microflows between coaxial cylinders," Phys. Rev. E **80**, 066317 (2009).
[50] P. Taheri and H. Struchtrup, "An extended macroscopic transport model for rarefied gas flows in long capillaries with circular cross section," Phys. Fluids **22**, 112004 (2010).
[51] P. Taheri, M. Torrilhon, and H. Struchtrup, "Couette and Poiseuille microflows: Analytical solutions for regularized 13-moment equations," Phys. Fluids **21**, 017102 (2009).
[52] M. Torrilhon and H. Struchtrup, "Regularized 13-moment-equations: Shock structure calculations and comparison to Burnett models," J. Fluid Mech. **513**, 171 (2004).
[53] M. Torrilhon and H. Struchtrup, "Boundary conditions for regularized 13-moment-equations for micro-channel flows," J. Comput. Phys. **227**, 1982 (2008).
[54] M. Torrilhon, "Convergence study of moment approximations for boundary value problems of the Boltzmann-BGK equation," Commun. Comput. Phys. **18**, 529 (2015).
[55] C. Truesdell and R. G. Muncaster, *Fundamentals of Maxwell's Kinetic Theory of a Simple Monatomic Gas* (Academic Press, 1980).
[56] M. Wakabayashi, T. Ohwada, and F. Golse, "Numerical analysis of the shear and thermal creep flows of a rarefied gas over the plane wall of a Maxwell-type boundary on the basis of the linearized Boltzmann equation for hard-sphere molecules," Eur. J. Mech., B: Fluids **15**, 175 (1996).
[57] W. Weiss, "Continuous shock structure in extended thermodynamics," Phys. Rev. E **52**, 5760 (1995).
[58] J. B. Young, "Calculation of Knudsen layers and jump conditions using the linearised G13 and R13 moment methods," Int. J. Heat Mass Transfer **54**, 2902 (2012).
[59] W. M. Zhang, G. Meng, and X. Wei, "A review on slip models for gas microflows," Microfluid. Nanofluid. **13**, 845 (2012).